HHS Public Access

Author manuscript

Alzheimers Dement. Author manuscript; available in PMC 2024 June 01.

Published in final edited form as:

Alzheimers Dement. 2023 June ; 19(6): 2355–2364. doi:10.1002/alz.12884.

Associations of phosphorylated tau pathology with whole-hemisphere ex-vivo morphometry in 7 tesla MRI

Shokufeh Sadaghiani[*,a], **Winifred Trotman**[a], **Sydney A Lim**[b], **Eunice Chung**[b], **Ranjit Ittyerah**[b], **Sadhana Ravikumar**[b,c], **Pulkit Khandelwal**[c], **Karthik Prabhakaran**[b], **Madigan L Lavery**[b], **Daniel T Ohm**[a], **Marianna Gabrielyan**[a], **Sandhitsu R. Das**[a], **Theresa Schuck**[d], **Noah Capp**[a], **Claire S Peterson**[a], **Elyse Migdal**[f], **Emilio Artacho-Pérula**[h], **María del Mar Arroyo Jiménez**[h], **Maria del Pilar Marcos Rabal**[h], **Sandra Cebada Sánchez**[h], **Carlos de la Rosa Prieto**[h], **Marta Córcoles Parada**[h], **Ricardo Insausti**[h], **John L Robinson**[d], **Corey McMillan**[a], **Murray Grossman**[a], **Edward B Lee**[d], **John A. Detre**[a], **Sharon X. Xie**[e], **John Q Trojanowski**[d,†], **M Dylan Tisdall**[b], **Laura EM Wisse**[a,b,g], **David J Irwin**[a], **David A. Wolk**[a], **Paul A. Yushkevich**[b]

[a]Department of Neurology, University of Pennsylvania, Philadelphia, PA 19104, USA

[b]Department of Radiology, University of Pennsylvania, Philadelphia, PA 19104, USA

[c]Department of Bioengineering, University of Pennsylvania, Philadelphia, PA 19104, USA

[d]Department of Pathology and Laboratory Medicine, University of Pennsylvania, Philadelphia, PA 19104, USA

[e]Department of Biostatistics, Epidemiology and Informatics, University of Pennsylvania, Philadelphia, PA 19104, USA

[f]College of Arts and Sciences, University of Pennsylvania, Philadelphia, PA 19104, USA

[g]Department of Diagnostic Radiology, Lund University, 22242 Lund, Sweden

[h]Human Neuroanatomy Laboratory, Neuromax CSIC Associated Unit, University of Castilla-La Mancha, Albacete, Spain

Abstract

INTRODUCTION.—Neurodegenerative disorders are associated with different pathologies that often co-occur but cannot be specifically measured by in vivo methods.

[*]Corresponding author: Shokufeh Sadaghiani, shokufeh.sadaghiani@pennmedicine.upenn.edu, Phone:215-573-8492, Goddard Laboratories 5th floor, 3710 Hamilton Walk, Philadelphia, PA 19104, USA.

[†]The author is deceased.

Author's contributions

S.S., S.R., L.E.M.W, D.A.W., P.A.Y., J.A.D., M.G., J.Q.T., S.R.D, P.K. and C.M. designed research; S.S., S.R., L.E.M.W., R.I., L.X., S.L., M.L.L., E.B.L., M.D.T., K.P., J.L.R., T.S., W.T., M.G., D.O., E.C., P.A.Y., N.C., C.S.P., E.M., E.A. P., M.M.A.J., M.P.M.R., S.C.S., C.R.P., M.C.P. and R.I. performed research; S.S., S.R., L.E.M.W., D.A.W., S.R.D., L.X and P.A.Y., R.I. and S.X.X. interpreted data and discussed results; S.S., S.R. and P.A.Y analyzed data and wrote the paper. S.S. was the principal designer and coordinator of the study and overviewed collection, analysis, and interpretation of the study data, with mentorship from P.A.Y., D.A.W., and J.A.D.

Ethics approval and consent to participate

Human brain specimens were obtained in accordance with the University of Pennsylvania Institutional Review Board guidelines. Where possible, pre-consent during life and, in all cases, next-of-kin consent at death was given.

METHODS.—Thirty-three brain hemispheres from donors with Alzheimer's disease (AD) spectrum diagnosis underwent T2-weighted MRI. Gray matter thickness was paired with histopathology from the closest anatomical region in the contralateral hemisphere.

RESULTS.—Partial Spearman correlation of phosphorylated tau and cortical thickness with TAR DNA-binding Protein 43 (TDP-43) and α-synuclein scores, age, sex and post-mortem interval as covariates showed significant relationships in entorhinal and primary visual cortices, temporal pole and insular and posterior cingulate gyri. Linear models including Braak stages, TDP-43 and α-synuclein scores, age, sex and post-mortem interval showed significant correlation between Braak stage and thickness in parahippocampal gyrus, entorhinal cortex and Broadman area 35.

CONCLUSION.—We demonstrated an association of measures of AD pathology with tissue loss in several AD regions despite limited range of pathology in these cases.

Keywords

Alzheimer's Disease; ex vivo MRI; neurodegeneration; biomarkers; cortical thickness

1. Introduction

Normal aging and neurodegenerative disorders are associated with a range of pathologies that often co-occur.(1) Heterogeneous pathologies are commonly observed in post-mortem studies of older brains(2–4) and they have been reported to have differential contributions to the pattern of cognitive impairment(5–8). Accordingly, only part of the variation in cognitive decline in neurodegenerative disorders such as Alzheimer's disease (AD) can be explained by the main features of its neuropathological definition.(9) Many of the pathologies observed in neurodegenerative disorders cannot be specifically detected or measured by in vivo methods. Nonetheless, successful identification of the topographic patterns of these pathologies in structural magnetic resonance imaging (MRI) may provide probabilistic, non-invasive biomarkers for their diagnosis, monitoring and treatment.

Although recent studies combining antemortem MRI and postmortem histopathological evaluation have improved our understanding of the relationship between neuropathology and in vivo MRI findings, such studies are uncommon and challenging to conduct. Research quality antemortem MRI scans are not always available and the heterogeneity of MRI protocols makes comparison between subjects challenging. Further, links between regions that are sampled for histology represent a small subset of the regions that can be measured with in vivo scans. Perhaps the greatest limitation is that antemortem imaging and postmortem assessment are often several years apart in most studies, such that some aspects of the pathology would not be present at time of the scan.(10)

Postmortem MRI is an alternative approach to studying pathology-structure relationships in the brain that does not suffer from a delay between image acquisition and pathological evaluation. Moreover, ex vivo MRI can be acquired using a consistent protocol that delivers higher spatial resolution and signal to noise ratio due to the much longer acquisitions that are minimally affected by motion artifacts as compared to in vivo MRI.(11–13)

Our goal was to design a study that can serve as a template linking specific patterns of tissue loss to underlying pathologies to provide insight into the interpretation of in vivo structural MRI studies in this population. In the present study, we investigated the association of gray matter thickness in cortical and medial temporal lobe (MTL) subregions measured from high-resolution 7 Tesla (7T) postmortem MRI and several common AD-related semi-quantitative neuropathology measures (regional phosphorylated tau (p-tau), regional neuronal loss, global Braak stage)(14) in a group of brain donors with AD spectrum diagnosis. The current analysis offers an extension to our prior work in which only MTL subregions imaged at 9.4T were investigated.(15)

2. Methods

2.1. Participants

Brain hemispheres of 33 donors were obtained from University of Pennsylvania Alzheimer's Disease Research Center (ADRC) and Frontotemporal Degeneration Center (FTDC). All participants provided consent to participate in research in ADRC or FTDC according to the University of Pennsylvania Institutional Review Board guidelines, and the next-of-kin provided autopsy consent. The cohort included a random mix of right and left hemispheres. All the brains included had primary or secondary neuropathological diagnoses of AD (based on the National Institute on Aging and Alzheimer's Association [NIA-AA] criteria)(16) or primary age-related tauopathy (PART) and did not show evidence of significant involvement with any other type of tauopathy or frontotemporal lobar degeneration with TAR DNA-binding protein 43 (TDP-43) inclusions (FTLD-TDP). Supplementary Table 1 provides a comprehensive description of primary, secondary and tertiary neuropathologies for each case.

2.2. Ex vivo MRI scanning

The MRI procedures for this study have been described previously.(17) Hemispheres were fixed in 10% formalin solution for at least 30 days, desiccated, and placed in a container of MRI-inert fluid (Fomblin) prior to imaging. Special care was taken to minimize air bubbles that would cause magnetic susceptibility artifacts. Images were obtained on Siemens MAGNETOM Terra 7 tesla scanner with a custom birdcage transmit/receive coil. The scanning protocol included a 3D-encoded T2-weighted sequence with 3 s repetition time (TR), 383 ms echo time (TE), turbo factor 188, echo train duration 951 ms, bandwidth 348 Hz/px with 4 averages, providing 0.3 mm^3 isotropic resolution in approximately 2 hours. (Fig. 1)

2.3. Gray Matter Thickness measurement

Eighteen cortical and MTL regions that largely encompassed areas typically sampled by neuropathologists for evaluation of AD pathology were examined.(18) Thirteen cortical regions outside of MTL included middle frontal gyrus, orbitofrontal gyrus, precentral gyrus (motor cortex), temporal pole, insular gyrus, inferior frontal gyrus (Broca's area), superior temporal gyrus, superior parietal lobule, angular gyrus, primary visual cortex (inside the calcarine sulcus), cingulate gyrus (anterior and posterior parts), the ventrolateral part of inferior temporal gyrus. Five MTL regions included entorhinal cortex, parahippocampal

gyrus, subiculum, Brodmann area 35 (BA35) and cornu ammonis 1 (CA1). (Fig. 2.A) The same approach developed and validated in our previously published work was used for cortical thickness measurement.(15, 19) Each region was manually marked with a dot consisting of few voxels on the MRI scan. Supplementary File 1 elaborates the guideline used to locate each region dot on MRI. A portion of surrounding grey matter extending 5–10 mm in all directions around each dot was semi-automatically segmented using the active contour segmentation in ITK-SNAP (version 3.8).(20) Thickness was then measured as the diameter of a maximally inscribed sphere, computed using Voronoi skeletonization(21), around the dot which is entirely contained in the segmentation. (Fig. 2.B) This semi-automated approach to measure cortical thickness was previously used and validated in Wisse at al.(15) to study thickness-pathology correlations in the medial temporal lobe.

2.4. Neuropathological evaluation

Neuropathological assessment was performed by expert neuropathologists at the University of Pennsylvania, based on previously established criteria and reported as standard semiquantitative scores.(18) The tissue specimens were embedded in paraffin blocks and cut into 6 μm sections. Immunohistochemistry evaluation was performed on contralateral hemisphere to the hemisphere scanned using previously validated antibodies and established methods:(22) NAB228 (monoclonal antibody [mAb], 1:8000, generated in the Center for Neurodegenerative Disease Research [CNDR]), phosphorylated tau PHF-1 (mAb, 1:1000, a gift from Dr. Peter Davies), TAR5P-1D3 (mAb, 1:500, a gift from Dr. Manuela Neumann and Dr. E. Kremmer) and Syn303 (mAb, 1:16,000, generated in the CNDR) to detect Aβ deposits, phosphorylated tau deposits, phosphorylated TDP-43 deposits and the presence of pathological conformation of α-synuclein, respectively. Each region was given a semiquantitative score between 0 (None) and 3 (Severe) for each specific pathology. Neuronal loss was visually assessed and reported as a semiquantitative score between 0 and 3. Fig. 3 shows samples of pathology slides used for semiquantitative rating of different pathologies and neuron loss. Sampled regions included occipital lobe, CA1/subiculum, amygdala, and middle frontal gyrus, cingulate, angular, superior/middle temporal and entorhinal gyri. For statistical analysis, gray matter thickness in each anatomical region measured on MRI was paired with neuropathology in either the exact (main regions) or the closest (exploratory regions) contralateral anatomical region for which semi-quantitative ratings were available. Supplementary Table 1 includes all MRI thickness measures and semi-quantitative pathology scores for each case.

We also conducted an exploratory analysis in which a quantitative measurement of p-tau tangle burden was extracted for each available digitally scanned PHF-1 histology slide by applying a machine learning technique. The details of this approach are in Supplementary File 2.

2.5. Statistical analysis

Analyses were performed in R (version 4.1.2). Sixteen regions with available thickness and paired pathological scores were included in the analysis. One-sided partial Spearman rank correlations was used to assess correlation of regional p-tau score with cortical thickness, and age, sex, post-mortem interval, regional TDP-43 and α-synuclein scores were used as

covariates. We also separately reported the Spearman correlation between semi-quantitative p-tau score and cortical thickness without any covariates.

We used the same statistical techniques to assess the correlation of grey matter thickness and exploratory quantitative p-tau tangle burden measures reported in Supplementary File 2.

In order to assess the correlation of Braak stage and cortical thickness, we used general linear model including age, sex, post-mortem interval, regional TDP-43 and α-synuclein scores. Because the distribution of Braak stages in our samples skewed towards more severe (see Table 1), Braak score was entered as a categorical variable with only two categories: “low/moderate” (stages 0-IV) and “severe” (stages V-VI).

One-sided Spearman correlation was also used to assess the correlation of regional neuron loss and cortical thickness.

The p-value threshold corresponding to the false discovery rate (FDR) of 0.05 was computed using the Benjamini and Hochberg method for multiple comparison correction (23), and statistical tests surviving this correction threshold are highlighted in the result section. However, other significant results that do not reach this stringent threshold are also reported, since there is strong prior data to support correlation of p-tau severity and thickness, and it is unlikely that statistical results with p-values below the 0.05 threshold but above the FDR threshold are spurious.

3. Results

The mean age of donors at death was 79.40±9.39 years (range, 63–99) and thirteen (40%) were female. The median Braak stage was V (range: II-VI). Table 1 summarizes the demographics and neuropathological characteristics of the brain donor cohort. Older subjects had lower Braak staging although the correlation between age and Braak stage was not statistically significant.

One-sided Spearman correlations between regional p-tau score and cortical thickness were significant in entorhinal cortex (r=−.58, *P* value=.0005, 27 d.f.), insular cortex (r=−.48, *P* value=.0021, 31 d.f.), temporal pole (r=−.45, *P* value=.0039, 31 d.f.), angular gyrus (r=−.43, *P* value=.0061, 31 d.f.), cingulate gyrus (posterior) (r=−.37, *P* value=.0169, 31 d.f.), superior parietal lobule (r=−.36, *P* value=.0207, 30 d.f.) and subiculum (r=−.35, *P* value=.0263, 30 d.f.). However, only insular and entorhinal cortices, temporal pole and angular gyrus met the more conservative FDR=0.05 threshold. (Table 2)

Partial Spearman correlations between regional semiquantitative p-tau scores and cortical thickness with age, sex, postmortem interval and regional TDP-43 and α-synuclein scores as covariates were significant in entorhinal cortex (r=−.57, *P* value=.0019, 23 d.f.), temporal pole (r=−.38, *P* value=.0219, 28 d.f.), insular gyrus (r=−.36, *P* value=.0318, 28 d.f.), subiculum (r=−.36, *P* value=.0348, 26 d.f.), posterior cingulate gyrus (r=−.34, *P* value=.039, 28 d.f.) and primary visual cortex (r=−.33, *P* value=.0413, 28 d.f.). (Table 2) However, only the entorhinal cortex meets the more conservative FDR=0.05 threshold. Fig. 4.A,

demonstrates scatter plots showing regional semiquantitative p-tau score versus cortical thickness in all 16 regions studied.

Supplementary File 2 contains the result from one-sided Spearman correlations of cortical thickness and regional quantitative p-tau tangle burden measure in either the exact (main regions) or the closest (exploratory regions) contralateral anatomical region for which quantitative measures were available.

Linear models including Braak stage (low/moderate=0-IV versus severe=V-VI), regional TDP-43 and α-synuclein scores, age, sex and post-mortem interval also showed significant correlations between Braak stage and cortical thickness in parahippocampal gyrus (t=−3.53; *P* value=.0016, 25 d.f.), entorhinal cortex (t=−2.33; *P* value=.0.0293, 22 d.f.) and BA35 (t=−2.2; *P* value=.0379, 23 d.f.). Only the parahippocampal gyrus met the more conservative FDR=0.05 threshold. Fig. 4.B, illustrates bar plots of Braak stage versus cortical thickness in all 16 regions studied.

Spearman correlations between regional neuronal loss score and cortical thickness were significant in insular gyrus (r=−.56, *P* value=.0003, 31 d.f.), entorhinal cortex (r=−.46, *P* value=.0067, 26 d.f.), cingulate gyrus (posterior) (r=−.43, *P* value=.0066, 31 d.f.), CA1 (r=−.40, *P* value=.0235, 24 d.f.), ventrolateral part of inferior temporal gyrus (r=−.38, *P* value=.0181, 29 d.f.), BA35 (r=−.35, *P* value=.0324, 27 d.f.), angular gyrus (r=−.34, *P* value=.0253, 31 d.f.), parahippocampal gyrus (r=−.31, *P* value=.0406, 31 d.f.) and temporal pole (r=−.30, *P* value=.0470, 31 d.f.). However, only insular and entorhinal cortices and posterior cingulate gyrus met the more conservative FDR=0.05 threshold. Supplementary Fig. 1, shows scatter plots illustrating the correlation between regional neuronal loss and cortical thickness.

4. Discussion

In the current study, we implemented a simple approach for obtaining gray matter thickness measurements from 7T ex vivo MRI scans in anatomical areas of interest and demonstrated the feasibility of using this approach to study pathology-thickness correlations in the whole brain. Our semi-automatic approach of measuring thickness at selected anatomical locations was previously validated in the MTL(15) and here it showed good inter-rater and intra-rater reliability.(24) We intended to provide an easy-to-implement approach for directly linking pathological and radiological measures of neurodegeneration. While in the future, reliable fully automated approaches for measuring cortical thickness on postmortem MRI, similar to tools like FreeSurfer(25), will likely be available for ex vivo MRI analysis, the ITK-SNAP based semi-automated approach used in this study is accessible now and not only offers a reliable and fast way to obtain thickness measurements in anatomical areas of interest but also provides necessary data for development and validation of automatic segmentation methods.(19)

The use of a commercial 7T human MRI scanner instead of the 9.4T animal MRI scanner in our prior MTL study may make our approach more accessible for other groups and eliminates the added uncertainty introduced by geometric distortions that occur when

scanning large samples on scanners intended for small animal imaging.(15) Another difference between this paper and our earlier MTL study,(15) which included a large number of FTLD diagnoses, is the more uniform postmortem cohort, limited to brain donors with an AD spectrum diagnosis. Focusing on just these cases makes our findings on tau-thickness and neurodegeneration-thickness correlations more relevant to AD research.

We investigated the correlation of regional p-tau pathology score and cortical thickness across 16 regions of interest (ROIs) and observed significant negative correlations within entorhinal cortex, temporal pole, insular gyrus, subiculum, posterior cingulate gyrus and primary visual cortex. This result is in agreement with previous antemortem(26–31) and postmortem(32) studies demonstrating the association of regional tau pathology and cortical thickness in AD and healthy subjects. The temporal pole has been reported to be among the cortical regions showing highest degree of thinning in early stages of AD and our results showing significant correlation of temporal pole thickness and regional p-tau are in concordance with that.(33–35). Only the correlation of entorhinal cortex thickness and regional p-tau score met the more conservative FDR=0.05 threshold for significance. The entorhinal cortex is one the earliest regions showing neurofibrillary tangle accumulation during the course of AD (36, 37), therefore stronger correlations in this region are expected. Surprisingly strong correlations with regional p-tau pathology were not detected for BA35, which includes the transentorhinal region, identified by Braak & Braak as the earliest site of AD tau pathology. However, in the exploratory data using quantitative measures of tau pathology, BA35 thickness did significantly correlate with the tangle burden score on the hippocampus slide, which includes BA35 (Supplementary File 2).

Our results also demonstrated a significant correlation between Braak staging and cortical thinning in ROIs, within the temporal lobe. This finding is consistent with the significant burden of tau pathology in these regions.(38) This is also in line with in vivo reports linking temporal region tau positron emission tomography (PET) uptake with cortical thickness on MRI.(26, 27) This result harmonizes with the notion of tau pathology in primary Braak regions playing an important role in cortical atrophy and subsequent cognitive decline during course of AD. Similar findings were reported by Whitwell et al. utilizing antemortem MRI and postmortem neuropathological evaluation, and grey matter loss was only observed in Braak stages V and VI and not III and IV.(39) They suggested that this conflict may be due to the non-quantitative nature of Braak staging, which mostly shows the pattern of involvement instead of the severity. Our dataset consisted of both low and high Braak stages.

Tau pathology has also been shown to be associated with neuronal loss in both AD and normal aging(40–42) and this loss of neurons is likely a key source of cortical thinning. (14) We observed that cortical thickness was significantly correlated with neuronal loss in multiple temporal lobe ROIs including temporal pole and entorhinal cortex, insular gyrus and cingulate gyrus (posterior) - the ROIs that showed significant correlation with p-tau pathology as well. This result is also consistent with the in vivo finding of tau pathology predicting the rate of future cortical thinning, particularly in temporal lobe regions.(26, 43, 44)

One limitation of our study is that although we excluded hemispheres with significant involvement with any other type of tauopathy or FTLD-TDP except AD, only a small number of cases had pure AD pathology and existence of co-pathologies was seen in majority of cases. The other limitation is that the pathology measures and MRI measures were obtained from contralateral hemispheres, potentially weakening observed associations, though pathology in AD is usually largely symmetrical between left and right hemispheres, (45, 46) making the likelihood of bias in these correlations low. A recent study examining correlations between automatically generated maps of MTL thickness and both contralateral and ipsilateral semiquantitative MTL tau pathology scores did not detect substantially different patterns of correlation.(47) In the future, we intend to carry out hemisphere-level thickness-pathology associations using histology sampled from the same hemisphere and same anatomical location as the MRI thickness measures, but this process is labor-intensive and the data are not available yet. Another potential limitation is the reliance on semi-quantitative measures of pathology, which are necessarily subjective and may not reflect the burden of pathology in a direct linear way. Our exploratory data in Supplementary File 2 found associations between quantitative tangle burden measures and cortical thickness that concur with the semiquantitative ratings, but also detected strong associations for BA35, which were not observed using semi-quantitative ratings. We presented these data as exploratory because the machine learning-based measures still need to be validated for the histology protocol used in this paper (6μm sections stained with PHF-1), and because they have limited anatomical specificity (i.e., the same “hippocampus slide tangle burden” measure captures pathology in the CA1, entorhinal cortex and BA35 regions). Future work will focus on addressing these limitations of our quantitative measures concurrent with obtaining histology from the same hemisphere as the MRI-based cortical thickness measures.(48, 49)

5. Conclusion

This study demonstrates an association of cortical and medial temporal lobe subregional thickness measured from postmortem MRI with semi-quantitative pathologic measures of AD pathology and local tissue loss in several common AD regions despite limited range of pathology in these cases. These initial results provide support for future work that will use larger datasets and more quantitative pathology measures to better describe the contribution of multiple pathologies to brain morphology in aging and neurodegenerative disease.

Supplementary Material

Refer to Web version on PubMed Central for supplementary material.

Acknowledgements

We gratefully acknowledge the tissue donors and their families. We also thank all the staff at the National Disease Research Interchange brain bank and at Center for Neurodegenerative Research (University of Pennsylvania) for performing the autopsies and making the tissue available for this project.

Funding

This work was supported in part by the National Institute of Health (Grants P30 AG072979, R01 AG056014, RF1 AG069474, R01 AG054519, P01 AG017586, P01AG066597, R01 NS109260) and Institute on Aging, University of Pennsylvania. The funding source had no involvement in conduct of the research and/or preparation of the article.

Competing interests

D.A.W has received grant support from Merck, Biogen, and Eli Lilly/Avid. D.A.W received consultation fees from Neuronix, Eli Lilly, Qynaps and is on the DSMB for a clinical trial run by Functional Neuromodulation. J.Q.T. received revenue from the sale of Avid to Eli Lilly as co-inventor on imaging related patents submitted by the University of Pennsylvania. D.J.I. is member of science advisory board of Denali Therapeutics. S.R.D. received consultation fees from Rancho Biosciences and Nia Therapeutics. The other authors have nothing to disclose.

References

1. Dugger BN, Dickson DW. Pathology of neurodegenerative diseases. Cold Spring Harbor perspectives in biology. 2017;9(7):a028035. [PubMed: 28062563]
2. Robinson JL, Lee EB, Xie SX, Rennert L, Suh E, Bredenberg C, et al. Neurodegenerative disease concomitant proteinopathies are prevalent, age-related and APOE4-associated. Brain. 2018;141(7):2181–93. [PubMed: 29878075]
3. Matej R, Tesar A, Rusina R. Alzheimer's disease and other neurodegenerative dementias in comorbidity: a clinical and neuropathological overview. Clinical biochemistry. 2019;73:26–31. [PubMed: 31400306]
4. Schneider JA, Arvanitakis Z, Bang W, Bennett DA. Mixed brain pathologies account for most dementia cases in community-dwelling older persons. Neurology. 2007;69(24):2197–204. [PubMed: 17568013]
5. Arvanitakis Z, Capuano AW, Leurgans SE, Bennett DA, Schneider JA. Relation of cerebral vessel disease to Alzheimer's disease dementia and cognitive function in elderly people: a cross-sectional study. The Lancet Neurology. 2016;15(9):934–43. [PubMed: 27312738]
6. Nag S, Yu L, Capuano AW, Wilson RS, Leurgans SE, Bennett DA, et al. Hippocampal sclerosis and TDP-43 pathology in aging and A lzheimer disease. Annals of neurology. 2015;77(6):942–52. [PubMed: 25707479]
7. Schneider JA, Boyle PA, Arvanitakis Z, Bienias JL, Bennett DA. Subcortical infarcts, Alzheimer's disease pathology, and memory function in older persons. Annals of neurology. 2007;62(1):59–66. [PubMed: 17503514]
8. Wilson RS, Yu L, Trojanowski JQ, Chen E-Y, Boyle PA, Bennett DA, et al. TDP-43 pathology, cognitive decline, and dementia in old age. JAMA neurology. 2013;70(11):1418–24. [PubMed: 24080705]
9. Boyle P, Yu L, Wilson R, Schneider J, Bennett DA. Relation of neuropathology with cognitive decline among older persons without dementia. Frontiers in Aging Neuroscience. 2013;5:50. [PubMed: 24058343]
10. Jagust WJ, Zheng L, Harvey DJ, Mack WJ, Vinters HV, Weiner MW, et al. Neuropathological basis of magnetic resonance images in aging and dementia. Annals of Neurology: Official Journal of the American Neurological Association and the Child Neurology Society. 2008;63(1):72–80.
11. Shatil AS, Matsuda KM, Figley CR. A method for whole brain ex vivo magnetic resonance imaging with minimal susceptibility artifacts. Frontiers in neurology. 2016;7:208. [PubMed: 27965620]
12. Augustinack JC, van der Kouwe AJ, Fischl B. Medial temporal cortices in ex vivo magnetic resonance imaging. Journal of Comparative Neurology. 2013;521(18):4177–88. [PubMed: 23881818]
13. Iglesias JE, Augustinack JC, Nguyen K, Player CM, Player A, Wright M, et al. A computational atlas of the hippocampal formation using ex vivo, ultra-high resolution MRI: application to adaptive segmentation of in vivo MRI. Neuroimage. 2015;115:117–37. [PubMed: 25936807]
14. Jellinger KA. Neuropathological assessment of the Alzheimer spectrum. Journal of Neural Transmission. 2020;127(9):1229–56. [PubMed: 32740684]

15. Wisse L, Ravikumar S, Ittyerah R, Lim S, Lane J, Bedard M, et al. Downstream effects of polypathology on neurodegeneration of medial temporal lobe subregions. acta neuropathologica communications. 2021;9(1):1–11. [PubMed: 33402227]
16. Jack CR Jr, Bennett DA, Blennow K, Carrillo MC, Dunn B, Haeberlein SB, et al. NIA-AA research framework: toward a biological definition of Alzheimer's disease. Alzheimer's & Dementia. 2018;14(4):535–62.
17. Tisdall MD, Ohm DT, Lobrovich R, Das SR, Mizsei G, Prabhakaran K, et al. Ex vivo MRI and histopathology detect novel iron-rich cortical inflammation in frontotemporal lobar degeneration with tau versus TDP-43 pathology. NeuroImage: Clinical. 2022;33:102913. [PubMed: 34952351]
18. Hyman BT, Phelps CH, Beach TG, Bigio EH, Cairns NJ, Carrillo MC, et al. National Institute on Aging–Alzheimer's Association guidelines for the neuropathologic assessment of Alzheimer's disease. Alzheimer's & dementia. 2012;8(1):1–13.
19. Khandelwal P, Sadaghiani S, Ravikumar S, Lim S, Arezoumandan S, Peterson C, et al. Gray Matter Segmentation in Ultra High Resolution 7 Tesla ex vivo T2w MRI of Human Brain Hemispheres. arXiv preprint arXiv:211007711. 2021.
20. Yushkevich PA, Pashchinskiy A, Oguz I, Mohan S, Schmitt JE, Stein JM, et al. User-guided segmentation of multi-modality medical imaging datasets with ITK-SNAP. Neuroinformatics. 2019;17(1):83–102. [PubMed: 29946897]
21. Ogniewicz RL, Ilg M, editors. Voronoi skeletons: theory and applications. CVPR; 1992.
22. Toledo JB, Van Deerlin VM, Lee EB, Suh E, Baek Y, Robinson JL, et al. A platform for discovery: the University of Pennsylvania integrated neurodegenerative disease biobank. Alzheimer's & dementia. 2014;10(4):477–84. e1.
23. Benjamini Y, Hochberg Y. Controlling the false discovery rate: a practical and powerful approach to multiple testing. Journal of the Royal statistical society: series B (Methodological). 1995;57(1):289–300.
24. Yushkevich PA, Piven J, Hazlett HC, Smith RG, Ho S, Gee JC, et al. User-guided 3D active contour segmentation of anatomical structures: significantly improved efficiency and reliability. Neuroimage. 2006;31(3):1116–28. [PubMed: 16545965]
25. Fischl B FreeSurfer. Neuroimage. 2012;62(2):774–81. [PubMed: 22248573]
26. LaPoint MR, Chhatwal JP, Sepulcre J, Johnson KA, Sperling RA, Schultz AP. The association between tau PET and retrospective cortical thinning in clinically normal elderly. Neuroimage. 2017;157:612–22. [PubMed: 28545932]
27. Harrison TM, Du R, Klencklen G, Baker SL, Jagust WJ. Distinct effects of beta-amyloid and tau on cortical thickness in cognitively healthy older adults. Alzheimer's & dementia. 2021;17(7):1085–96.
28. Xia C, Makaretz SJ, Caso C, McGinnis S, Gomperts SN, Sepulcre J, et al. Association of in vivo [18F] AV-1451 tau PET imaging results with cortical atrophy and symptoms in typical and atypical Alzheimer disease. JAMA neurology. 2017;74(4):427–36. [PubMed: 28241163]
29. Mak E, Bethlehem RA, Romero-Garcia R, Cervenka S, Rittman T, Gabel S, et al. In vivo coupling of tau pathology and cortical thinning in Alzheimer's disease. Alzheimer's & Dementia: Diagnosis, Assessment & Disease Monitoring. 2018;10:678–87.
30. Das SR, Xie L, Wisse LE, Vergnet N, Ittyerah R, Cui S, et al. In vivo measures of tau burden are associated with atrophy in early Braak stage medial temporal lobe regions in amyloid-negative individuals. Alzheimer's & Dementia. 2019;15(10):1286–95.
31. Whitwell JL, Graff-Radford J, Tosakulwong N, Weigand SD, Machulda MM, Senjem ML, et al. Imaging correlations of tau, amyloid, metabolism, and atrophy in typical and atypical Alzheimer's disease. Alzheimer's & Dementia. 2018;14(8):1005–14.
32. Frigerio I, Boon BD, Lin C-P, Galis-de Graaf Y, Bol J, Preziosa P, et al. Amyloid-β, p-tau and reactive microglia are pathological correlates of MRI cortical atrophy in Alzheimer's disease. Brain communications. 2021;3(4):fcab281.
33. Dickerson BC, Bakkour A, Salat DH, Feczko E, Pacheco J, Greve DN, et al. The Cortical Signature of Alzheimer's Disease: Regionally Specific Cortical Thinning Relates to Symptom Severity in Very Mild to Mild AD Dementia and is Detectable in Asymptomatic Amyloid-Positive Individuals. Cerebral Cortex. 2008;19(3):497–510. [PubMed: 18632739]

34. Arnold SE, Hyman BT, Van Hoesen GW. Neuropathologic Changes of the Temporal Pole in Alzheimer's Disease and Pick's Disease. Archives of Neurology. 1994;51(2):145–50. [PubMed: 8304839]
35. Herlin B, Navarro V, Dupont S. The temporal pole: From anatomy to function—A literature appraisal. Journal of Chemical Neuroanatomy. 2021;113:101925. [PubMed: 33582250]
36. Braak H, Braak E. Demonstration of amyloid deposits and neurofibrillary changes in whole brain sections. Brain pathology. 1991;1(3):213–6. [PubMed: 1669710]
37. Van Hoesen GW, Hyman BT, Damasio AR. Entorhinal cortex pathology in Alzheimer's disease. Hippocampus. 1991;1(1):1–8. [PubMed: 1669339]
38. Braak H, Alafuzoff I, Arzberger T, Kretzschmar H, Del Tredici K. Staging of Alzheimer disease-associated neurofibrillary pathology using paraffin sections and immunocytochemistry. Acta neuropathologica. 2006;112(4):389–404. [PubMed: 16906426]
39. Whitwell J, Josephs K, Murray M, Kantarci K, Przybelski S, Weigand S, et al. MRI correlates of neurofibrillary tangle pathology at autopsy: a voxel-based morphometry study. Neurology. 2008;71(10):743–9. [PubMed: 18765650]
40. Gómez-Isla T, Hollister R, West H, Mui S, Growdon JH, Petersen RC, et al. Neuronal loss correlates with but exceeds neurofibrillary tangles in Alzheimer's disease. Annals of Neurology: Official Journal of the American Neurological Association and the Child Neurology Society. 1997;41(1):17–24.
41. Dawe RJ, Bennett DA, Schneider JA, Arfanakis K. Neuropathologic correlates of hippocampal atrophy in the elderly: a clinical, pathologic, postmortem MRI study. PloS one. 2011;6(10):e26286. [PubMed: 22043314]
42. Ohm DT, Fought AJ, Martersteck A, Coventry C, Sridhar J, Gefen T, et al. Accumulation of neurofibrillary tangles and activated microglia is associated with lower neuron densities in the aphasic variant of Alzheimer's disease. Brain Pathology. 2021;31(1):189–204. [PubMed: 33010092]
43. Xie L, Das SR, Wisse LE, Ittyerah R, Yushkevich PA, Wolk DA, et al. Early tau burden correlates with higher rate of atrophy in transentorhinal cortex. Journal of Alzheimer's Disease. 2018;62(1):85–92.
44. La Joie R, Visani AV, Baker SL, Brown JA, Bourakova V, Cha J, et al. Prospective longitudinal atrophy in Alzheimer's disease correlates with the intensity and topography of baseline tau-PET. Science translational medicine. 2020;12(524):eaau5732.
45. King A, Bodi I, Nolan M, Troakes C, Al-Sarraj S. Assessment of the degree of asymmetry of pathological features in neurodegenerative diseases. What is the significance for brain banks? Journal of neural transmission. 2015;122(10):1499–508. [PubMed: 26021735]
46. Stefanits H, Budka H, Kovacs GG. Asymmetry of neurodegenerative disease-related pathologies: a cautionary note. Acta Neuropathologica. 2012;123(3):449–52. [PubMed: 22222584]
47. Ravikumar S, Wisse LEM, Lim S, Ittyerah R, Xie L, Bedard ML, et al. Ex vivo MRI atlas of the human medial temporal lobe: characterizing neurodegeneration due to tau pathology. Acta Neuropathologica Communications. 2021;9(1):173. [PubMed: 34689831]
48. Yushkevich PA, Muñoz López M, Iñiguez de Onzoño Martin María M, Ittyerah R, Lim S, Ravikumar S, et al. Three-dimensional mapping of neurofibrillary tangle burden in the human medial temporal lobe. Brain. 2021;144(9):2784–97. [PubMed: 34259858]
49. Ravikumar S, Wisse L, Lim S, Irwin D, Ittyerah R, Xie L, et al., editors. Unfolding the Medial Temporal Lobe Cortex to Characterize Neurodegeneration Due to Alzheimer's Disease Pathology Using Ex vivo Imaging 2021; Cham: Springer International Publishing.

Highlights

- Neurodegenerative disorders are associated with co-occurring pathologies which cannot be specifically measured by in vivo methods.
- Identification of the topographic patterns of these pathologies in structural magnetic resonance imaging (MRI) may provide probabilistic biomarkers.
- We demonstrated the correlation of the specific patterns of tissue loss from ex-vivo brain MRI with underlying pathologies detected in post-mortem brain hemispheres in patients with Alzheimer's disease (AD) spectrum disorders.
- The results provide insight into the interpretation of in vivo structural MRI studies in patients with AD spectrum disorders.

Research in context

Systematic review. The authors reviewed the literature using traditional methods like PubMed. Although recent studies combining antemortem magnetic resonance imaging (MRI) and postmortem histopathological evaluation have improved our understanding of the relationship between neuropathology and in vivo MRI findings, they are challenging to conduct and using post-mortem MRI as an alternative approach has not been fully studied. The relevant citations are appropriately cited.

Interpretation. Our result demonstrates an association of semi-quantitative measures of Alzheimer's disease (AD) pathology with local tissue loss in several common AD regions.

Future directions. This study provides support for future studies that will use larger datasets and more quantitative pathology measures to better describe the contribution of multiple pathologies to brain morphology in aging and neurodegenerative disease.

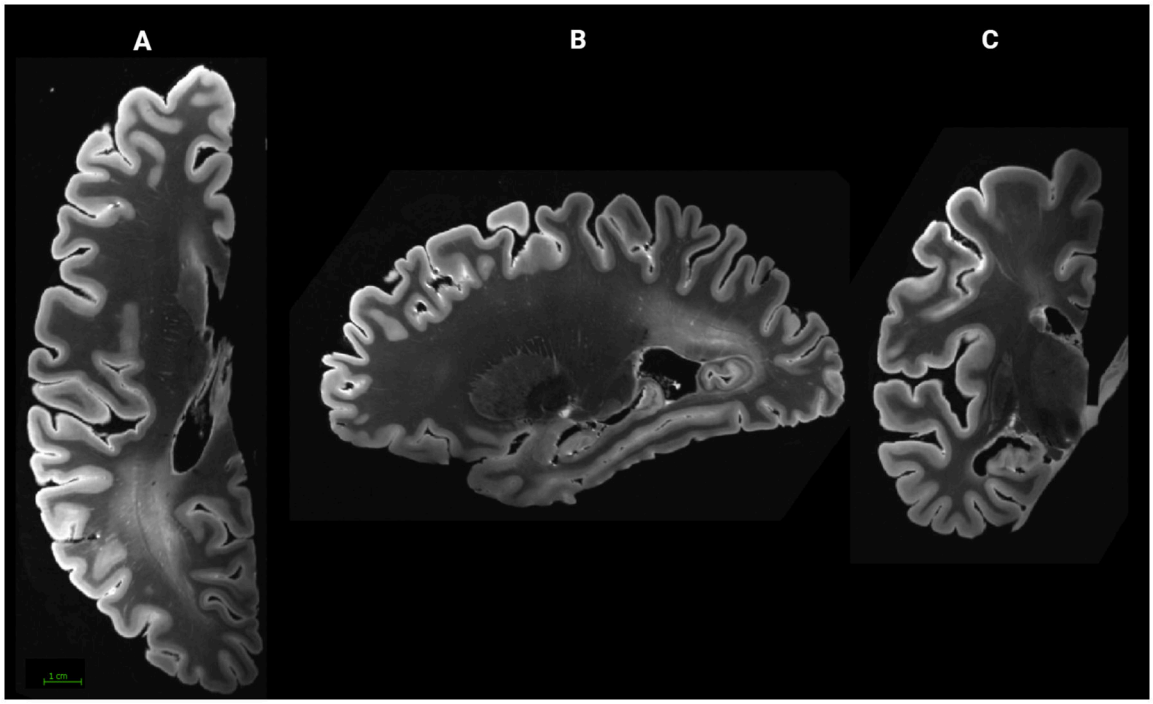

Figure 1.

Ex-vivo Magnetic Resonance Image of one hemisphere. (A) axial, (B) sagittal, and (C) coronal slices. Created with BioRender.com

*Color should be used for Fig. 1 in print.

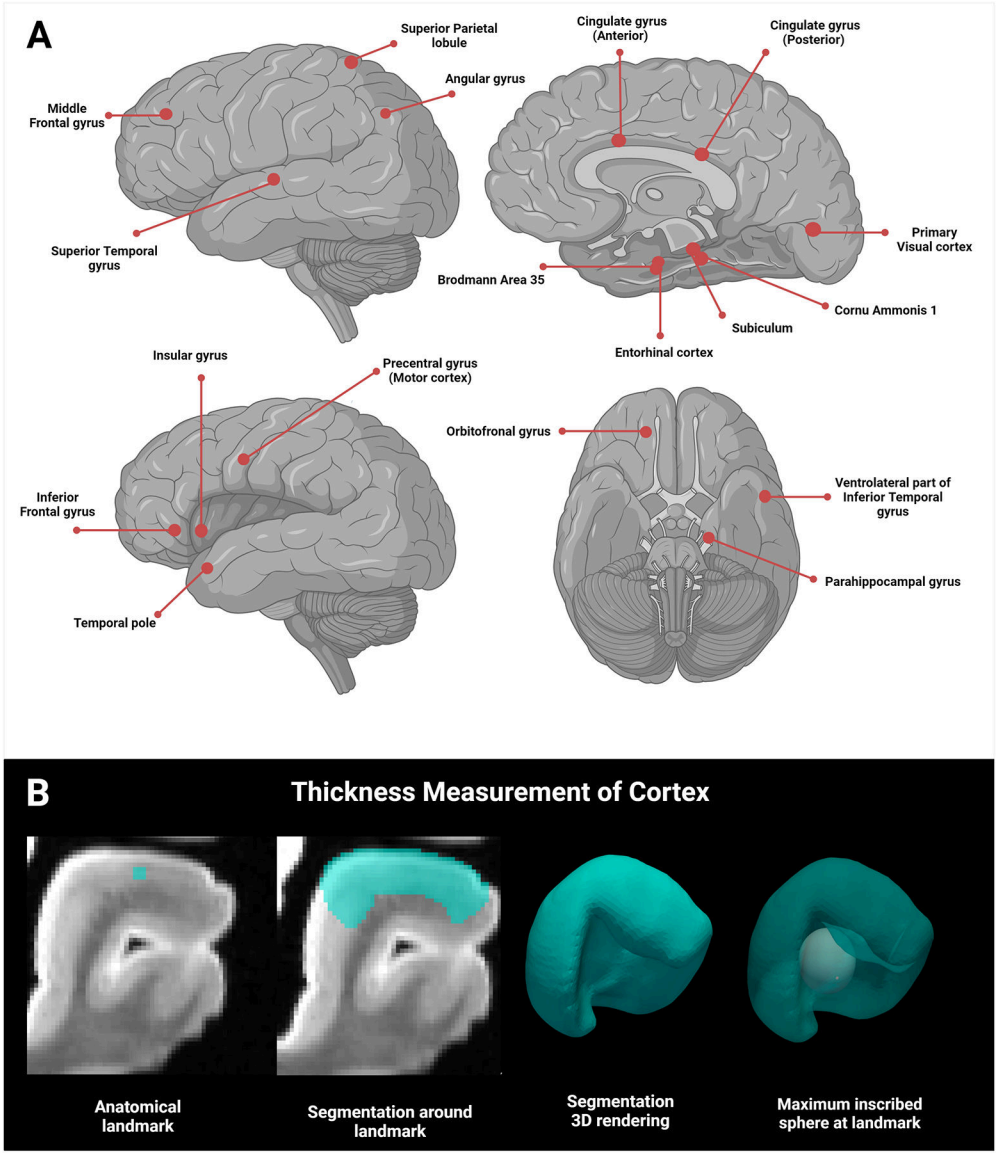

Figure 2.

Local regional cortical thickness measurement locations and pipeline. (A) Approximate dot location for individual cortical regions. (B) Cortical thickness is measured at the 18 landmarks shown, but statistical analyses are performed for 16 regions except Motor cortex and Orbitofrontal cortex. This is due the fact that currently we do not have neuropathological data for these two regions. [20] A dot (shown: the superior temporal gyrus cortex dot) is first placed to define an anatomical landmark, around which a semi-automatic level set segmentation of the surrounding cortical ribbon is provided. A maximally inscribed sphere is then computed using Voronoi skelentonization [21] and the diameter of the sphere gives thickness at that landmark. Created with BioRender.com

*Color should be used for Fig. 2 in print.

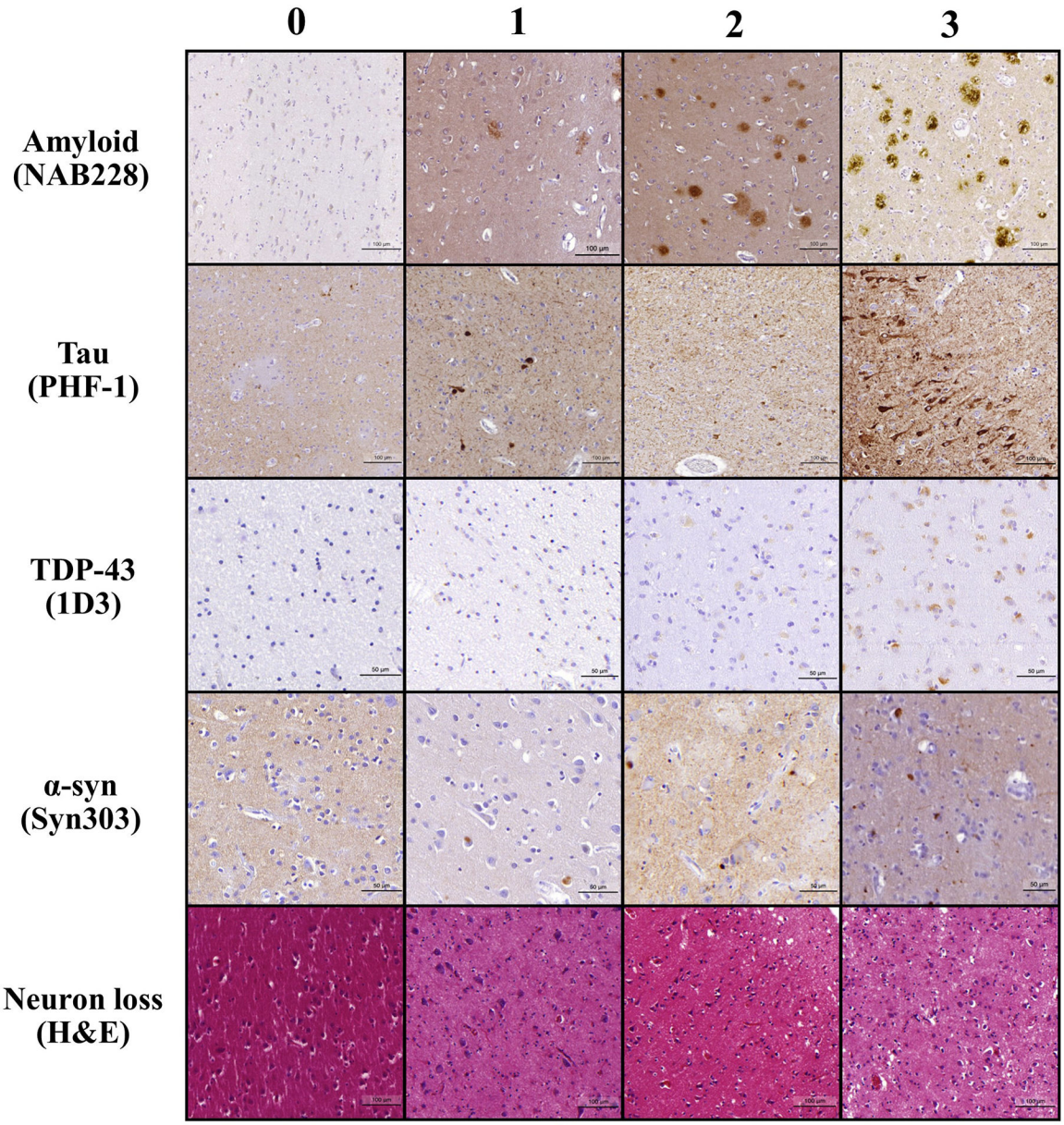

Figure 3.

Examples of pathological assessment for each regional pathology. The columns are severity ratings (left to right): 0–3. The rows from top to bottom show amyloid plaques (NAB228 antibody), tau pathology (PHF-1 antibody), TDP-43 inclusions (pS409/410 antibody), Lewy bodies (Syn303 antibody) and neuron loss (Hematoxylin & Eosin staining) in different cortical and medial temporal lobe regions included in the current work. Scale bars are shown.

*Color should be used for Fig. 3 in print.

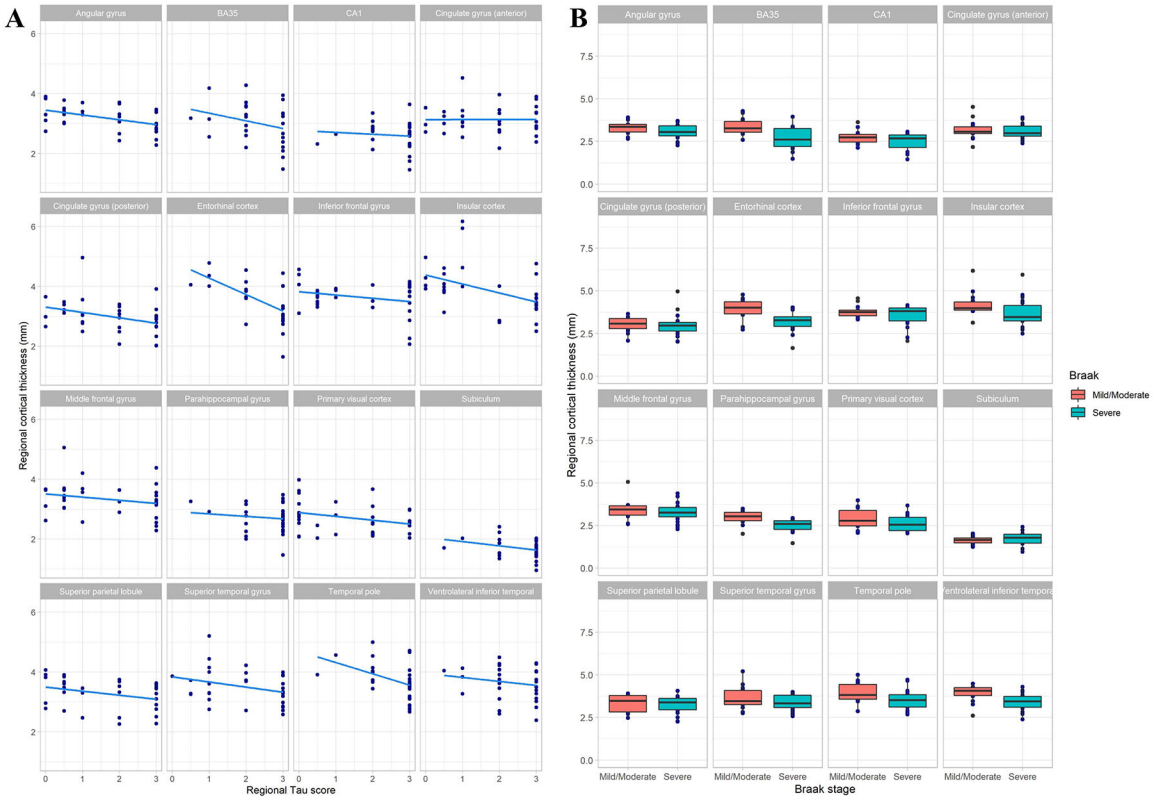

Figure 4.

(A) Scatter plots showing thickness measurements versus regional semiquantitative tau scores. Linear regression fit is shown. The one-sided Spearman correlations with age, sex, post-mortem interval and regional TDP-43 and α-synuclein scores as covariates were significant in entorhinal cortex, insular gyrus, subiculum, posterior cingulate gyrus and primary visual cortex ($p<0.05$). (B) Thickness measurements versus Braak stage. The p-value of the model including age, sex, post-mortem interval and regional TDP-43 and α-synuclein scores was significant in Parahippocampal gyrus, entorhinal cortex and BA35 ($p<0.05$).

*Color should be used for Fig. 4 in print.

Table 1.

Demographic composition of the brain donor cohort, primary, secondary and tertiary postmortem neuropathological diagnoses and global neuropathological scoring. Neuropathological measures are derived from contralateral hemisphere to the hemisphere scanned.

Brain donor cohort		
N	33	
Age	79.40±9.39	63–99
Sex	13 F, 20 M	
Scanned hemisphere	16 R, 17 L	
Post-mortem interval (hours)	19.77±13.26	
Neuropathological diagnosis		
	Primary	Secondary/tertiary
Alzheimer's disease	23	7
Lewy body disease	8	14
PART	1	2
Cerebrovascular disease	1	3
LATE		10
Chronic Traumatic Encephalopathy		3
Hippocampal Sclerosis		1

Global neuropathological staging				
	0	**1**	**2**	**3**
Amyloid (A)	3	2	4	24
Braak (B)	0	4	10	19
CERAD (C)	5	4	5	19

Six-stage Braak scheme	**0**	**1**	**2**	**3**	**4**	**5**	**6**
	0	0	4	6	4	3	16

Abbreviations: PART, primary age-related tauopathy; LATE, Limbic-predominant Age-related TDP-43 Encephalopathy; CERAD, Consortium to Establish a Registry for Alzheimer's Disease.

Table 2.

Correlation coefficients and p-values from one-sided Spearman correlation and partial Spearman correlation of regional semi-quantitative tau score and cortical thickness with age, sex, post-mortem interval and regional semi-quantitative TDP43 and α-synuclein scores as covariates. (A) Main regions with paired thickness and histopathology scores. (B) Exploratory regions in close proximity to the regions with available corresponding neuropathology score.

MRI region of interest	Corresponding Pathology region of interest	Correlation coefficient (p-value) of Spearman correlation between structure and local p-tau burden	Correlation coefficient (p-value) of partial Spearman correlation between structure and local p-tau burden
A			
Entorhinal cortex	Entorhinal cortex	−0.58 (0.0005) *	−0.57 (0.0019) *
Subiculum	Cornu ammonis 1/subiculum	−0.35 (0.0263) *	−0.36 (0.0348) *
Primary visual cortex	Occipital gyrus	−0.27 (0.0622)	−0.33 (0.0413) *
Angular gyrus	Angular gyrus	−0.43 (0.0061) *	−0.31 (0.0519)
Superior temporal gyrus	Superior/middle temporal gyrus	−0.23 (0.1009)	−0.28 (0.071)
Middle frontal cortex	Middle frontal gyrus	−0.21 (0.1167)	−0.24 (0.1136)
Cornu ammonis 1	Cornu ammonis 1/subiculum	−0.09 (0.3224)	0.07 (0.3925)
B			
Temporal pole	Amygdala	−0.45 (0.0039) *	−0.38 (0.0219) *
Insular gyrus	Middle frontal gyrus	−0.48 (0.0021) *	−0.36 (0.0318) *
Cingulate gyrus (Posterior)	Cingulate gyrus	−0.37 (0.0169) *	−0.34 (0.039) *
Superior parietal lobule	Angular gyrus	−0.36 (0.0207) *	−0.31 (0.0561)
Brodmann area 35	Entorhinal cortex	−0.24 (0.1029)	−0.22 (0.1488)
Ventrolateral part of inferior temporal gyrus	Entorhinal cortex	−0.15 (0.2106)	−0.07 (0.3616)
Cingulate gyrus (Anterior)	Cingulate gyrus	0.03 (0.5659)	−0.02 (0.4505)
Parahippocampal gyrus	Cornu ammonis 1/subiculum	−0.09 (0.3156)	−0.01 (0.4824)
Inferior frontal	Middle frontal gyrus	−0.10 (0.2917)	0.09 (0.3311)

* Significant p-values.